Analyzing buzzer-acquired physically-modelled data for FWI

Wong, J., Henley, D.C., and Innanen, K.A.H.

ABSTRACT

We acquired physically-modelled seismic data within a homogeneous volume of water using piezoelectric buzzer transducers as sources and receivers. The recorded signals exhibited laboratory frequencies in the range 40kHz to 100kHz. After scaling, we obtained common-source seismograms with frequencies in the range 4Hz to 10Hz. The scaled frequencies are suitable for efficient full waveform inversion (FWI) in the seismic exploration world. However, the observed source/receiver wavelets are very long, and they are different for every source-receiver position. Both factors cause the buzzer-acquired seismic data to be ill-suited for efficient FWI imaging. We investigated time-domain filtering techniques for decreasing the time durations of the source/receiver wavelets and increasing the uniformity of their codas.

INTRODUCTION

We wish to demonstrate whether or not the University of Calgary Seismic Physical Modelling Facility (Wong et al., 2009) could be used to produce seismic data suitable for efficient full-waveform inversion (FWI) imaging. Efficient FWI imaging requires seismic data with dominant frequencies in the 4Hz to 10Hz range. To obtain scaled seismograms with such low frequencies, we resorted to using piezoelectric buzzers immersed in water as a source and a receiver. The buzzer-acquired data possessed the desired frequencies, but the signal waveforms were too variable with changing source/receiver positions and the time-durations of the signal codas were too long to be ideally suited for efficient FWI. In this article, we report initial results from using a convolution filtering technique in time domain to decrease the time-durations of the source/receiver signals and to minimize their variability with changing source/receiver positions. In the Appendix, we compare buzzer-acquired data and piezopin-acquired data and their ability to detect a relatively small target.

METHOD

Small piezoelectric buzzers are Helmholtz resonators designed to produce relatively low ultrasonic frequencies. Immersed in water, the buzzers produce and detect signals with laboratory frequencies in the range 40-100 kHz that scale down to seismic frequencies of 4-10Hz. The specific transducers we used to produce the low-end ultrasonic frequencies are Murata PKM13EPYH4002-B0 buzzers. See Figure A1(b).

We inserted the transducers into a homogeneous volume of water (acoustic velocity of 1485 m/s). and recorded a set of transmission seismograms across a 2D circular plane with diameter of approximately 30cm (3000m scaled). Wong et al. (this volume) described the acquisition procedure in detail. The resulting data were archived in the SEGY file **bzzr_No_Target_40db.sgy**. Figure 1 shows the scaled positions of the sources and receivers in the XY plane and a selection of rays traversing the circular area being scanned. Figure 2(a) shows the raypaths joining the source with receivers for an example common-source gather (CSG) from the file.

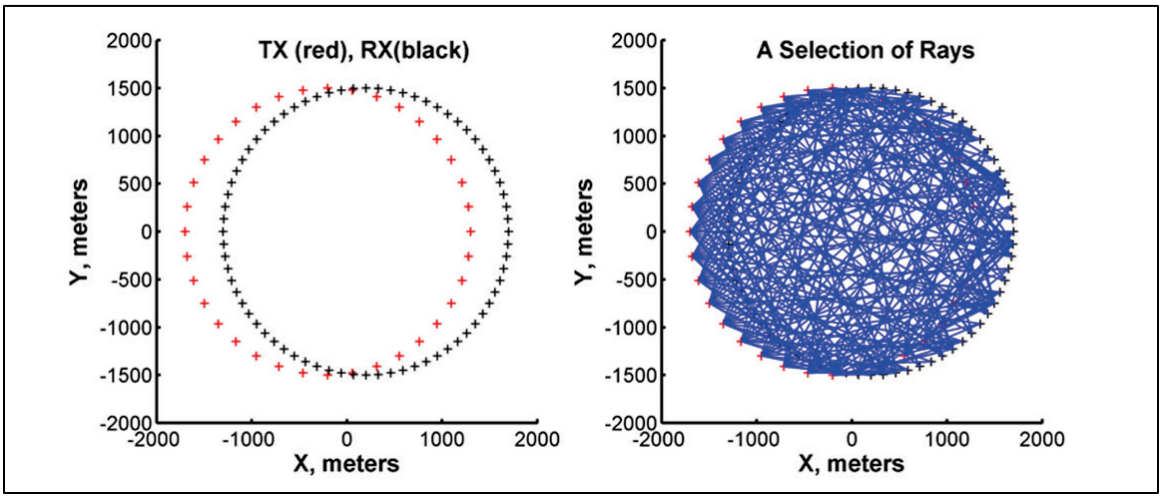

Fig. 1. Acquisition geometry. Left: Location of sources (red) and receivers (black). Right: Raypaths joining sources and receivers (only every fifth raypath is shown).

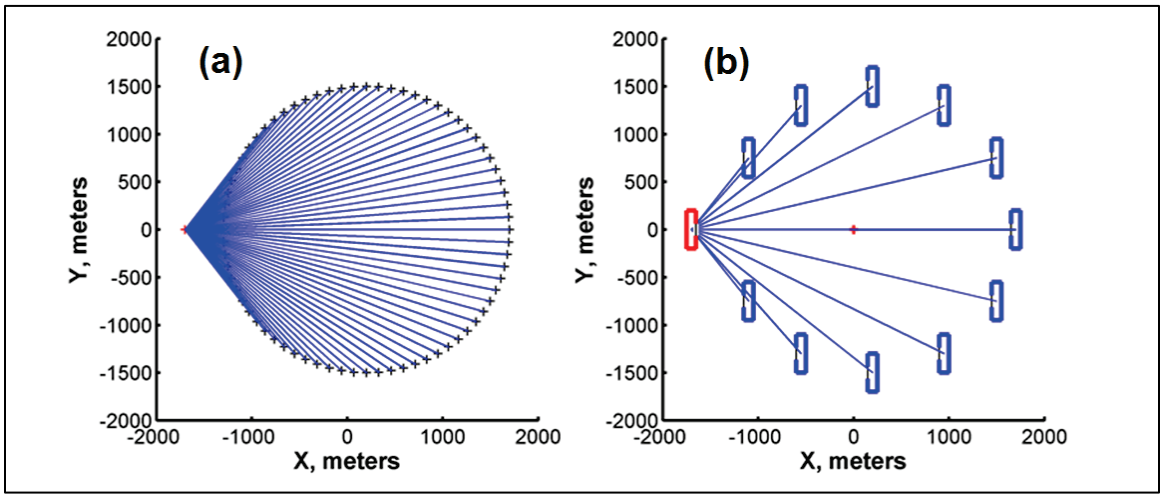

Fig. 2. (a) Raypaths for an example CSG. (b) Schematic showing the radially asymmetric footprints in the XY plane of source (red) and receiver (blue) buzzers.

The buzzers were mounted on and attached to the positioning subsystem of the Physical Modelling Facility in such a way that gave the rectangular footprints in the XY plane shown on Figure 2(b). Relative to their centers, the transducer footprints are not radially symmetric, and this asymmetry gives rise to asymmetric radiation and reception patterns in the XY plane. Therefore, as source and receiver positions shift, we expect varying mismatches in the radiation/reception patterns to affect waveform uniformity.

The SEGY file **bzzr_No_Target_40db.sgy** contains 37 CSGs. Each CSG consists of 1, 5, 9, …69, 73, 69, …9, 5, or 1 distinct seismograms for a total of 1333 traces. Each trace is 3072 samples long digitized at intervals of 1ms. The scaled source-receiver XY coordinates recorded in the SEGY trace headers are in units of meters times 10.

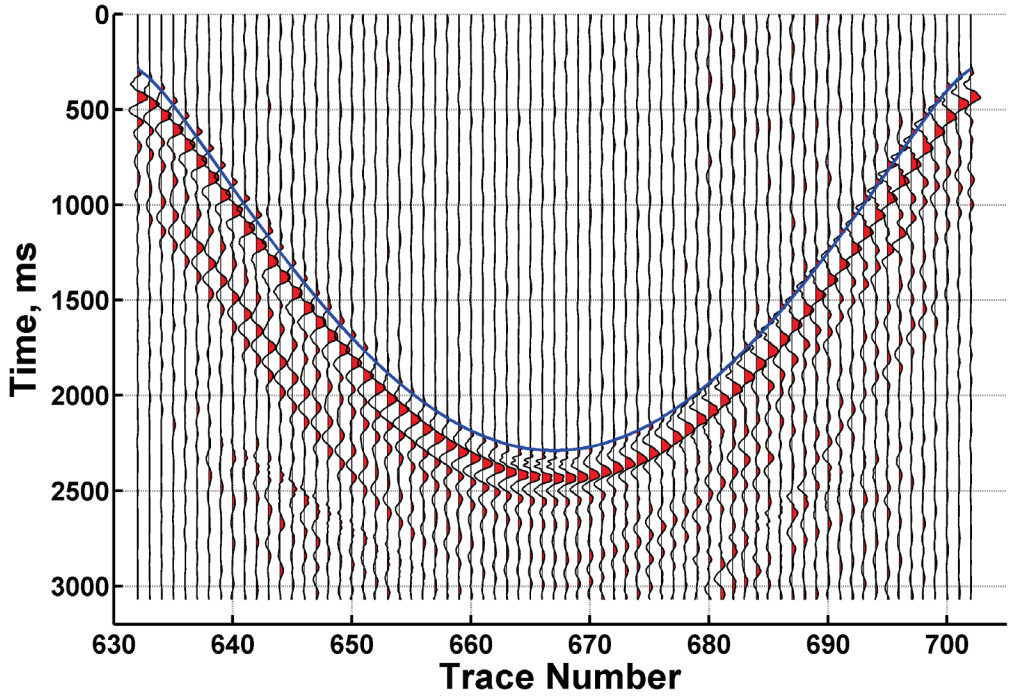

Fig 3. Trace-normalized seismograms through the homogeneous water medium. The trace numbers denote different receiver positions. The blue line marks calculated water arrival times.

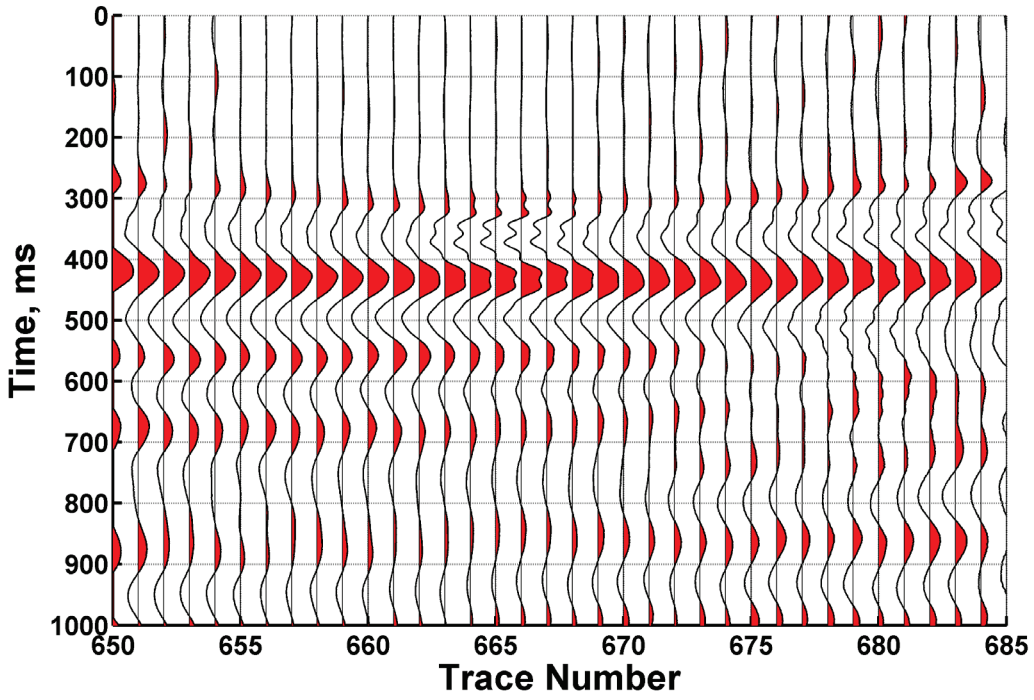

Fig. 4. Traces aligned to the minimum water arrival time on Figure 3. Note the long-duration codas and lack of symmetry with respect to the apex position (Trace Number 667).

Figure 3 shows the seismograms from the example CSG. The blue line marks the water arrival time based on ray lengths determined from the source-receiver coordinates saved on the SEGY trace headers. Figure 4 displays the traces flattened to the minimum water arrival time on Figure 3. Every trace is different because of transducer asymmetries in the XY plane. The asymmetries are a result of the way they were mounted on the gantries of the positioning subsystem (see Figure 2b). The geometric asymmetries cause position-dependent mismatches in asymmetric radiation/reception patterns resulting in the variations in the observed waveforms. The differences are exacerbated by significant self-scattering due to the large transducer sizes (relative to dominant wavelengths).

Since the transmission seismograms were recorded through a homogeneous medium, we may consider them to be "source" wavelets. The average of the aligned traces on Figure 4 gives us an estimated "source" wavelet shown on Figure 5. The spectrum of the average trace indicates that seismic data acquired with buzzer transducers have energy in the 4-10Hz range sufficient for efficient FWI imaging. However, the traces on Figures 3 and 4 are too long and too variable with receiver position to be ideally suited for use in efficient FWI procedures. In what follows, we attempt to compress the long durations and make the waveforms stationary with receiver position.

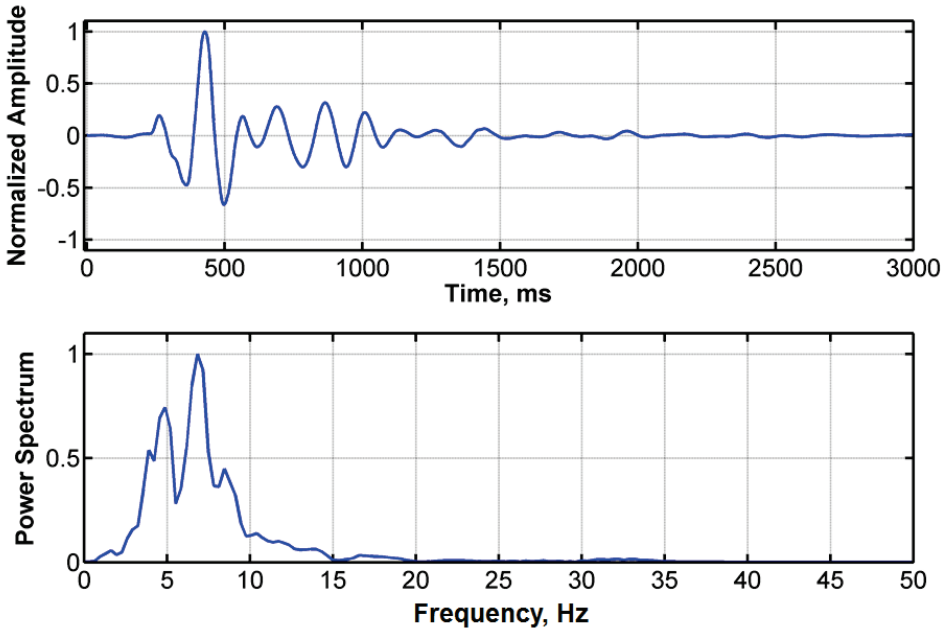

Fig 5. Average of the aligned traces on Figure 4 and its spectrum.

Deriving a source wavelet from non-stationary seismic traces

We can manipulate the raw traces on Figure 1 to obtain a derived wavelet that is both shorter in length and more consistent with receiver position. We first apply bandpass filtering and windowing to obtain the CSG of shortened traces plotted on Figure 6. Then we flatten the shortened traces as is shown on Figure 7, and form the average. The time-shifted and polarity-reversed average trace plotted on Figure 8 (bottom) can be considered to be a "source" wavelet derived entirely from the observed raw seismograms.

The derived source wavelet is compared to the theoretical minimum-phase wavelet plotted on Figure 8 (top) that was used in a successful numerical test of efficient FWI imaging. The similarities suggest that the substituting the experimentally determined wavelet for the theoretical wavelet in the numerical test of FWI would pose no problems.

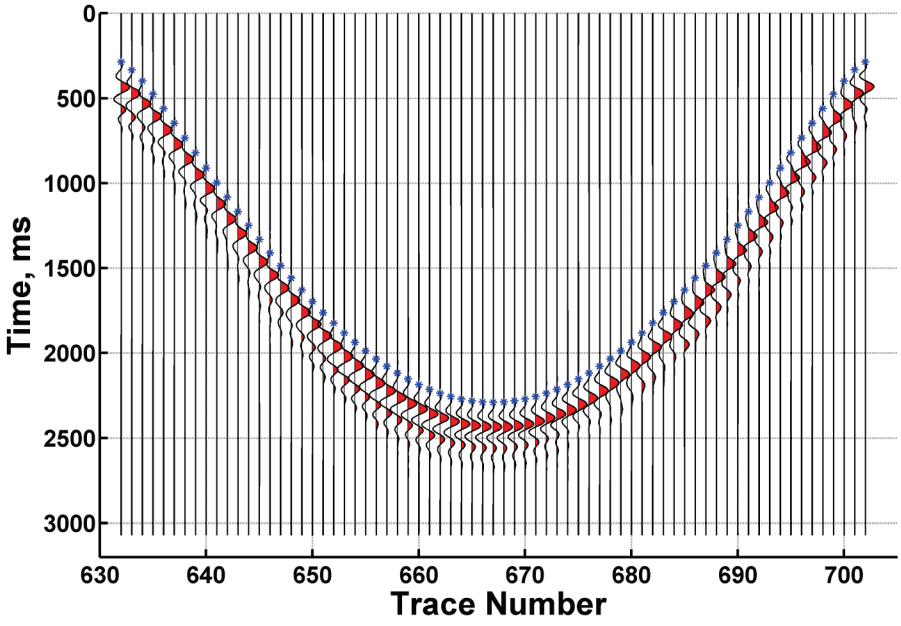

Fig. 6. Traces of Figure 1 after bandpass filtering and windowing. Ormsby band filter parameters are [0.2 1.0 10 20] Hz. Window width parameters are [0 150 250 400] ms, with tapered ends.

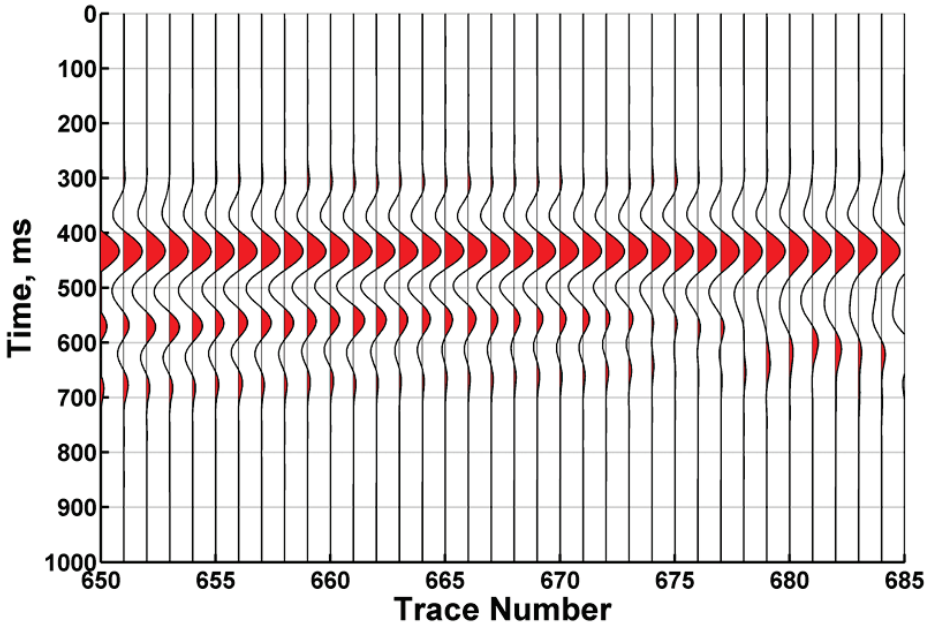

Fig. 7. Windowed traces from Figure 6 flattened to water-arrival times, and then trimmed aligned to first-peak times.

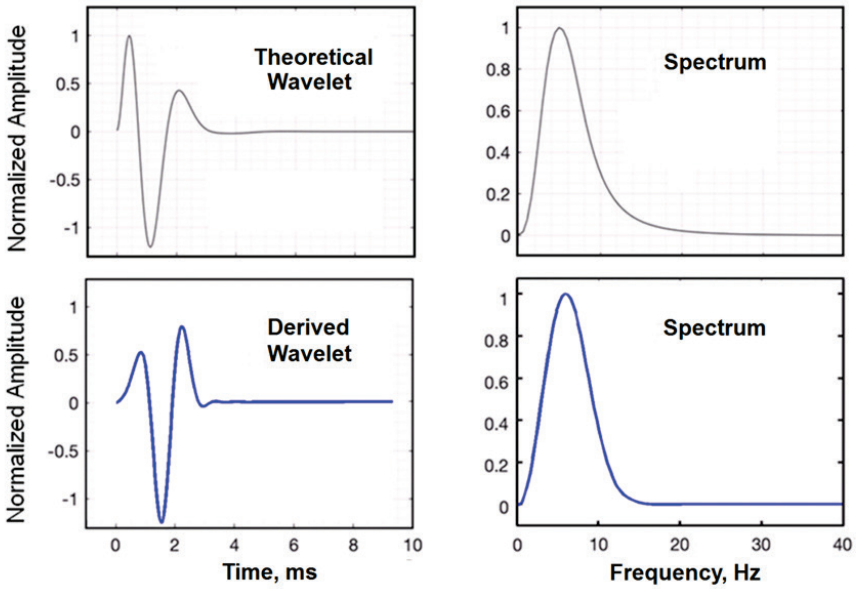

Fig. 8. Top: Theoretical source wavelet and its spectrum, used in a numerical test of FWI. Bottom: Time-shifted and polarity-reversed average of the traces on Figure 7 and its spectrum.

Transforming the raw long-duration seismograms in Time Domain

We can transform the raw long-duration "source" wavelets on Figure 3 so that they are copies of the derived source wavelet shown on figure 5. We consider each raw seismic trace to be a time-delayed distorted source wavelet. Therefore, we shift them so that the first-breaks occur near zero time as shown on Figure 9(a). Each long-duration trace on Figure 9(a) can be regarded as an input trace into a trace-transforming procedure whose desired output is the derived source wavelet on Figure 5 (bottom).

Let $S_j^{in}(\omega)$ and $S^{out}(\omega)$ be the fast Fourier transforms of the input signals $s_j^{in}(t)$ and the desired trace $s^{out}(t)$, respectively. Define a frequency-domain filter $F_j(\omega)$ by

$$F_j(\omega) = \frac{S^{out}(\omega)}{S_j^{in}(\omega) * conj\left(S_j^{in}(\omega)\right)} * conj\left(S_j^{in}(\omega)\right), \qquad (1a)$$

if $S_j^{in}(\omega) > 0.001 * \max\left(S_j^{in}(\omega)\right)$; otherwise, set

$$F_j(\omega) = 0\ . \qquad (1b)$$

Then

$$S^{out}(\omega) = F_j(\omega) * S_j^{in}(\omega) \qquad (2)$$

will be a near identity. For practical purposes, we wish to do the trace transformation in time domain. Thus, we apply an inverse FFT to the frequency-domain filter $F_j(\omega)$ to get its time-domain equivalent $f_j(t)$.

Finally, in time domain, we have

$$s^{out}(t) = f_j(t) \times s_j^{in}(t) \qquad (3)$$

where × represents the convolution operator.

Figure 9(a) shows the raw seismograms of Figure 3 flattened to calculated water arrival times and shifted so the first breaks are near zero time. They are input to be transformed by the procedure defined by Equations 1 to 3. Figure 9(b) shows the results after time-domain filtering using Equation 3.

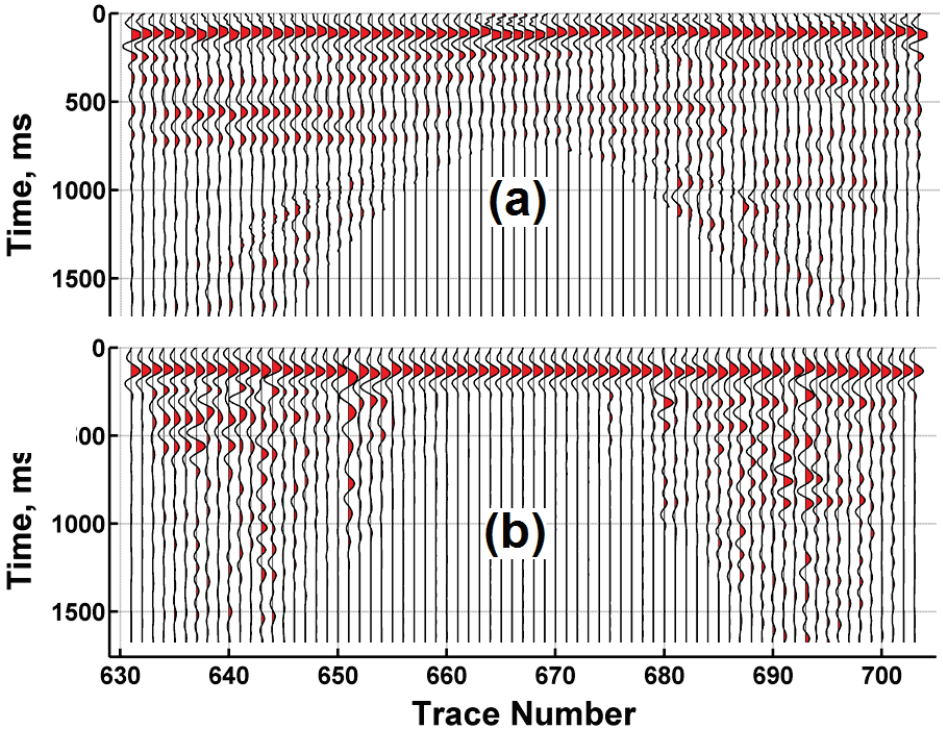

Fig. 9. Using a time-domain filtering technique to convert long-duration, non-stationary signals to short-duration, more uniform wavelets: (a) Input signals. (b) Output signals. Present results show promise, but the method needs to be modified to handle input traces that do not convert well.

Figure 9 indicates that the time-domain filtering technique in its present form yields mixed results. It worked very well for some input traces (e.g., traces near the left and right edges of Figure 9, and 10 traces on either side of Trace Number 667), converting them to excellent replicas of the desired source wavelet.

However, the method failed for other input traces, yielding outputs that are very poor copies of the desired source wavelet. The common feature of traces that converted poorly seems to be the presence of discernible amplitudes past about 700ms. We are hopeful that future modifications to the filtering technique can be found to improve the performance for those traces.

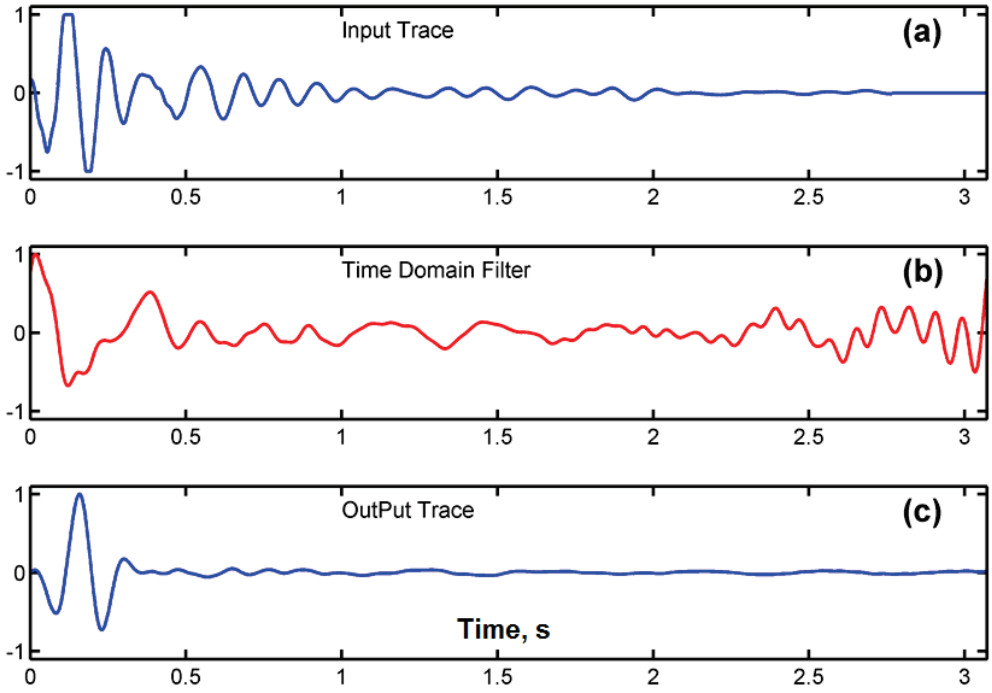

Fig. 10. (a) The input trace (first trace on Figure 9a). (b) The time-domain filter associated with the input trace. (c) The well-compressed output trace after convolution.

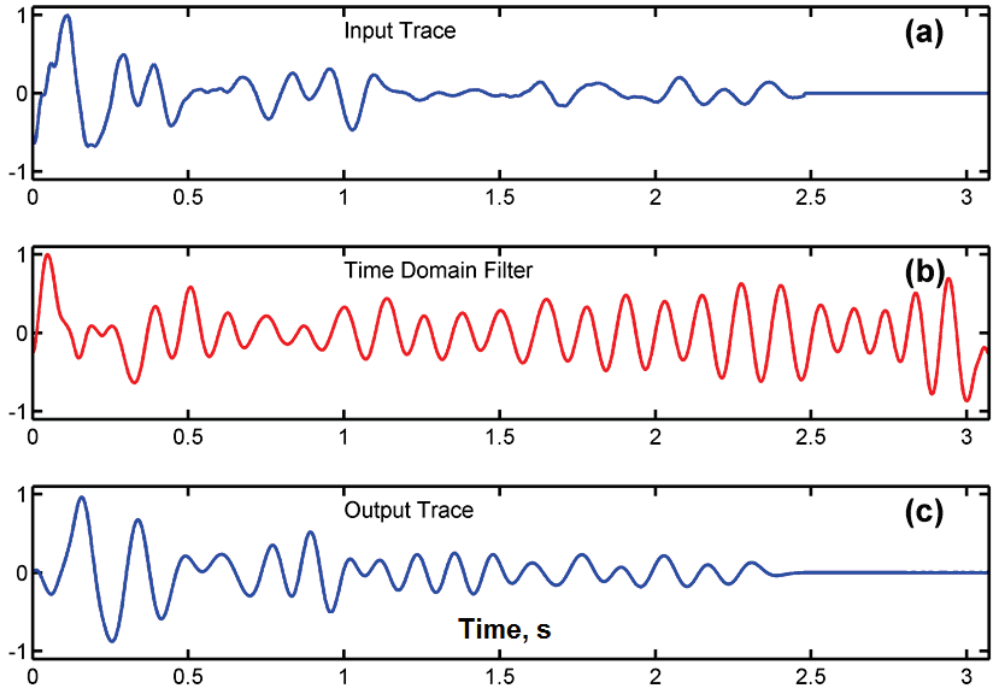

Fig. 11. (a) The input trace (fifth trace on Figure 9a). (b) The time-domain filter associated with the input trace. (c) The poorly-compressed output trace after convolution.

We examine the convolution results more closely. Figure 10(a) is a plot of the first trace on Figure 9(a), Figure 10(b) is its time-domain filter $f_j(t)$, and Figure 10(c) is the output after convolution. For this input trace, the conversion is deemed to be successful, since the output trace is very similar to the desired source wavelet shown on the bottom of Figure 8. Figure 11 similarly plots the result for another input trace for which the output trace is not well compressed.

The time-domain filters and the output traces associated with the two example input traces look very different. We will investigate the differences between input traces and the associated time-domain filters and hopefully find modifications to the time-domain filtering technique that will improve its poor performance for traces that convert poorly. One thing is clear already: we must decrease the raw signal time durations by increasing the damping of the resonance effects generated by the buzzers.

SUMMARY AND DISCUSSION

Small piezoelectric buzzers are Helmholtz resonators that produce relatively low ultrasonic frequencies in the range 40-100 kHz when they are immersed in water. Resonance results in undesirable long-duration signal codas. A buzzer has a diameter of 13mm, which is a significant fraction of the dominant wavelengths of 20 to 38 mm. Because of the relatively large transducer sizes compared to the dominant wavelengths, transducer self-scattering adds undesirable secondary arrivals to be mixed in with the "pure" source signature.

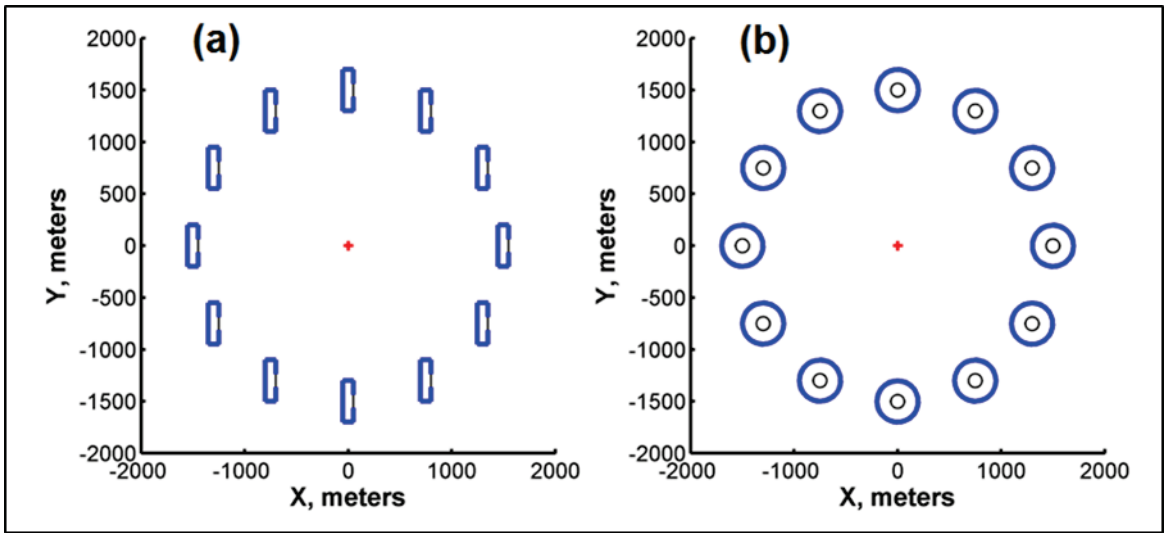

Fig. 12. Footprints of buzzers on the XY plane for two mounting methods. (a) Orientation with buzzer rotational axes pointing in the Y direction (used for the present acquisition). (b) Orientation with buzzer rotational axes pointing in the Z-direction.

The results in this report were acquired using a transducer mounting method that resulted in the rectangular and radially asymmetric transducer footprints on the XY plane shown on Figure 12(a). The radially asymmetric footprints mean that the radiation and reception patterns of the buzzer transducers do not have point source/receiver symmetry.

Symmetric radiation/reception patterns would result if an alternative mounting method were used to give the footprints shown on Figure 12(b). In this case, we expect that the variation of trace codas with changing source and receiver positions would be much reduced. For this reason, we will re-do the entire experiment using this alternative mounting method.

CONCLUSION

We recorded physical model transmission seismograms in water using 70kHz piezoelectric buzzers as sources and receivers. The observed dominant frequencies were in the range 4Hz to 10Hz after applying the physical-model scaling factor of 10^4. These frequencies are suitable for efficient FWI imaging, but the raw source/receiver wavelets are much too long and much too variable to be ideal for FWI. The undesirably long-duration codas are due to (under-damped) resonance within the buzzers.

We attempted to find a suitable time-domain filtering technique to compress the raw observed wavelets and simultaneously increase their consistency as receiver position change. Our initial construction of time-domain filters gave mixed results. Some raw traces converted to well-compressed, consistent replicas of the desired source wavelet, but other raw traces converted very poorly. Increased damping of the resonances in signals produced and detected by the buzzers to decrease the time durations would significantly improve the performance of the time-domain filtering method.

Future research involves searching for a way to damp the buzzer resonance mechanically and finding modifications to the time-domain filters that perform poorly. In addition, we will acquire transmission data using buzzer mounting methods that give a circular footprint in the XY plane. We expect that these steps will lead to better performing time-domain filters. The improved filters can be used with the Arbitrary Waveform Generator (Wong et al., 2020) to drive the buzzers and yield the consistent, short-duration, and stationary source signatures needed for efficient FWI.

ACKNOWLEDGEMENT

We thank the sponsors of CREWES for continued support. This work was funded by CREWES industrial sponsors and NSERC (Natural Science and Engineering Research Council of Canada) through the grant CRDPJ 543578-19.

REFERENCES

Henley, D. C., 2021, Preliminary processing of physical modeling data from circular arrays: CREWES Research Report, Vol. 33, no.14.

Wong, Joe, Kevin W. Hall, Eric V. Gallant, Rolf Maier, Malcolm B. Bertram, and Don C. Lawton, 2009, Seismic Physical Modelling at the University of Calgary: CSEG Recorder, vol. 34, no.3. Mar 2009 | VOL. 34 No. 03 | View Issue

Wong, J., Bertram, K. L., Zhang, H., Hall, K. W., and Innanen, K. A. H., 2020, Enhanced source hardware and tank for physical modelling: *CREWES Research Report*, **32**, 55, 24.

Wong, J., Henley, K., and Innanen, K. A. H., 2021, Acquiring physically-modeled seismic data using 70kHz piezoelectric buzzers, CREWES Research Report, Vol. 33, no.48.

APPENDIX: COMPARING PIEZOPIN DATA AND BUZZER DATA

We compare physically-modelled transmission seismograms acquired with piezopin transducers with seismograms acquired with buzzer transducers. The two types of transducers are shown on Figure A1. Acting as ultrasonic sources and receivers in water, the piezopins produce wavelets with laboratory frequencies of about 500kHz (Wong et al., 2009), while the buzzer-generate wavelets have laboratory frequencies near 72kHz. These laboratory-measured values scale down to seismic-world values of 50Hz and 7.2Hz, respectively. The factor-of-seven difference in dominant frequencies and wavelengths means that FWI imaging with buzzer-acquired data would require significantly less computational time than with piezopin-acquired data.

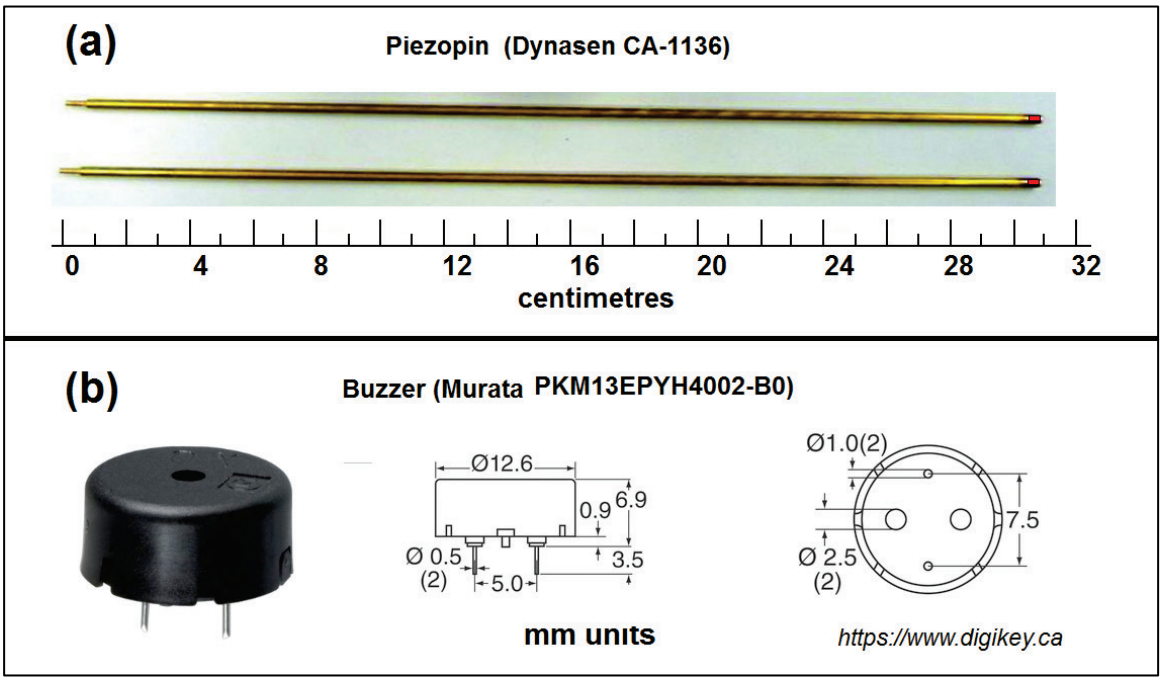

Fig. A1. Transducers used for physical modeling. (a) The diameters of the piezopins are 2.36mm. The active piezoelectric elements are located within the tips shown in red. (b) Buzzers act as Helmholtz resonators. The active elements are benders (thin piezoelectric wafers bonded to thin brass discs) located within the PVC housing.

We acquired physically-modelled seismic data across a circular area on an XY plane within water. Piezopin transducers were used as source and receiver placed at locations similar to those shown on Figure 1, and a PVC target was placed inside the circle circumference. Individual vertically stacked seismograms 3072ms long digitized with 1ms sampling intervals were recorded by driving the piezopin source with 200V pulses repeatedly 100 times. The complete dataset for this survey is archived in the SEGY file **pzpCirc15_PVCTarget.sgy** and contains 1333 seismograms grouped into 37 CSGs.

Figure A2 is a plot of the seismic traces for 10 different CSGs from the dataset. The displayed CSGs have been flattened from the water arrival times observed on

seismograms acquired in the homogeneous (no targets) medium. Amplitudes were adjusted in such a way as to highlight the anomalies caused by the presence of the target. The travel time and amplitude anomalies on the figure reveal the presence of the target.

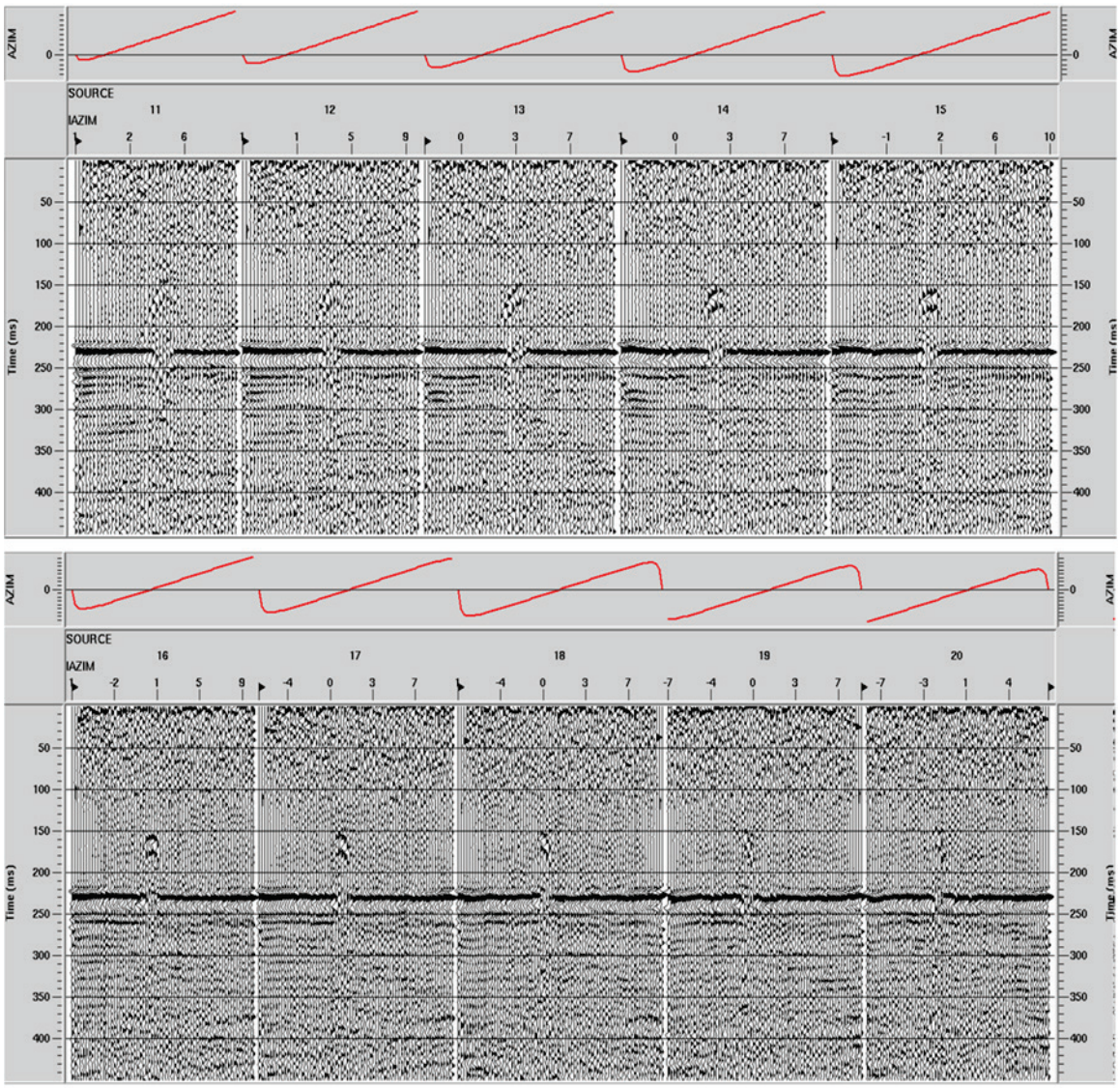

Fig. A2. AGC display of piezopin-acquired transmission seismograms for ten CSGs from the file pzpCirc15_PVCTarget.sgy. All traces have been flattened to water first-break time

.

Henley (this volume) analyzed this dataset in order to roughly define the location and size of the PVC target by back-projecting the amplitude/slowness anomalies observed on the CSGs. The hope was that by using a starting velocity model with the geometry of the PVC target roughly defined, the computation burden of obtaining a more detailed and accurate image of the target using FWI would be reduced significantly. The back-projection technique is depicted schematically on Figure A3. The figure shows that, for the simple case of a single target in a homogeneous medium, the intersection of all rays exhibiting anomalous travel times and/or anomalous amplitudes roughly locates the target and gives its approximate size.

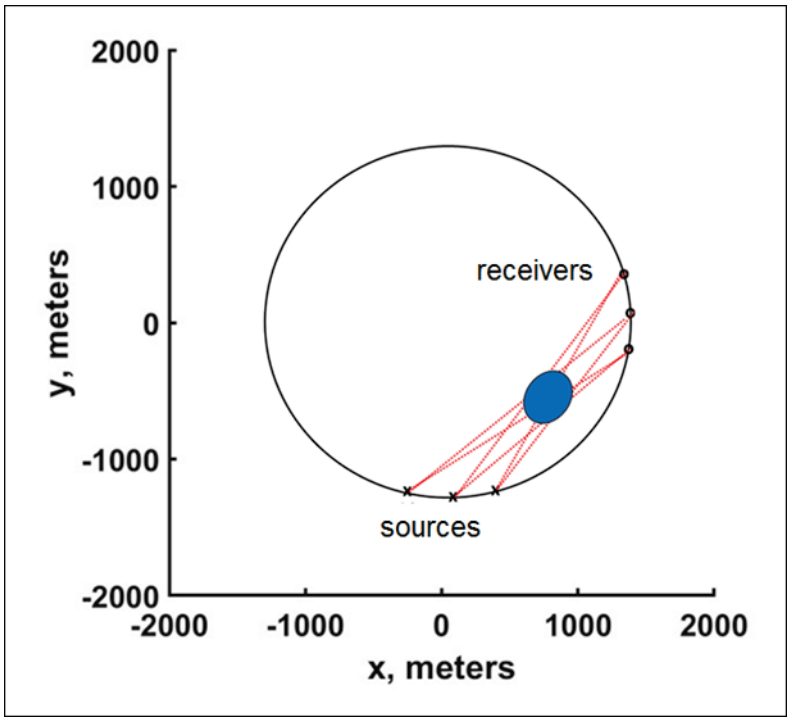

Fig. A3. Schematic diagram representing straight-ray back-projection of anomalous amplitudes or anomalous slowness values. The intersection of all rays with anomalies would approximately determine the location and size of a single target within the scanned 2D area.

Although the target was detected on all CSGs plotted on Figure A2, we see that the signal-to-noise ratios (SNRs) are low. We repeated the experiment using vertical stacking of 400 and higher pulse voltage of 400V driving the piezopin sources, once without any targets within the scanned area, and again including two targets. The data are archived in the files **pzp_No_Target_40dB.sgy** and **pzp_TwoTarget_40dB.sgy**. Figure A4 shows CSGs from the two resulting datasets with all seismograms flattened to the calculated direct arrival times through water.

The two-target experiment was repeated again using buzzer transducers for the source and receiver. The data are archived in the files **bzzr_No_Target_40dB.sgy** and **bzzr_TwoTarget_40dB.sgy**. The results shown on Figure A5 can be compared directly with those on Figure A4. Note the difference in time scales or the two figures.

The observed dominant frequency for the buzzer data is about 7.2Hz, seven times lower than the 50Hz for the piezopin data. Visually, the buzzer seismograms detect the two targets with less resolution and in different ways. More detailed analysis of why the targets affect the high-frequency piezopin-acquired data and the low-frequency buzzer-acquired data differently is beyond the scope of this report.

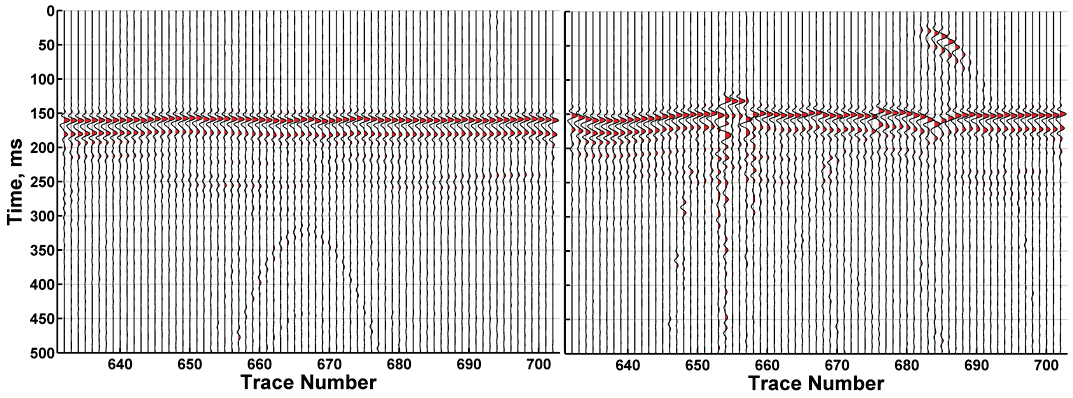

Fig. A4. Two CSGs recorded using piezopin transducers with acquisition geometry similar to that of Figure 1. Traces have been flattened to the water first break times. Left: For the case without any targets. Right: for the case with two targets (the RHS target is a solid PVC hemisphere; the LHS target is a PVC ring filled with water).

.

.

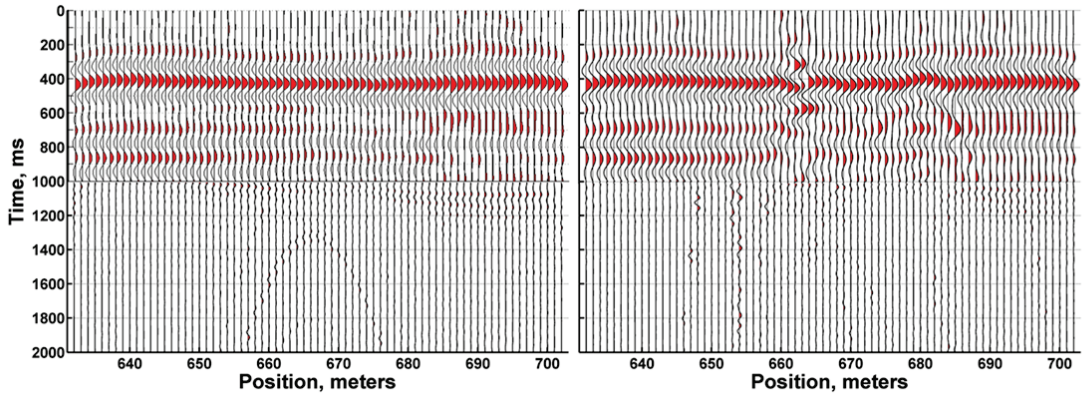

Fig. A5. Two flattened CSGs recorded using buzzer transducers with acquisition geometry similar to that used for recording the data on Figure A4. Left: For the case without any targets. Right: for the case with two targets. The targets for this figure have been displaced slightly from those for Figure A4.